Dyes and Pigments 196 (2021) 109779

Contents lists available at ScienceDirect

Dyes and Pigments

journal homepage: www.elsevier.com/locate/dyepig

Self-assembled quinoxaline derivative: Insight into disaggregation induced selective detection of nitro-aromatics in aqueous medium and live cell imaging

Megha Basak [a], Basu Bhattacharjee [b], Aiyagari Ramesh [b], Gopal Das [a,*]

[a] Department of Chemistry, Indian Institute of Technology Guwahati, Assam, 781039, India
[b] Department of Biosciences and Bioengineering, Indian Institute of Technology Guwahati, Assam, 781039, India

ARTICLE INFO

Keywords:
Quinoxaline
Self-assembly
Explosives
Analyte-induced disassembly
Host-guest interaction

ABSTRACT

Advancement in fluorescent chemosensor for discriminative and precise detection of picric acid (PA) in aqueous medium is highly desirable owing to its alarming impact on the natural environment via soil and groundwater pollution. To this end, we have successfully fabricated a quinoxaline-based receptor (**Probe 1**) to detect PA in 100% aqueous medium. **Probe 1** self-assembled to form leaf-like structures in pure water as micro aggregates (~940 nm) and transformed entirely into smaller spherical shape (~354 nm) upon addition of PA. DFT analysis and lifetime experiment validated that both PET and FRET from the electron-rich **Probe 1** to electron-deficient PA are concurrently responsible for effective fluorescence quenching. The self-assembled probe exhibited excellent selectivity towards PA (K_{sv} of 22.6 × 10^6 M^{-1}) with a ~56 ppb detection limit. Importantly, PA detection on solution-coated paper strips was achieved at the picogram level. Furthermore, to evaluate the practical usefulness, the probe has been used to detect PA in actual water and soil samples. Interestingly, **Probe 1** was non-toxic to cultured HeLa cells and rendered detection of intracellular picric acid through live cell imaging.

1. Introduction

Detection of trace explosives have gained imperative attention in the past few decades to mitigate counter-terrorism, homeland defense, environmental pollution, and forensic interrogation [1–3]. Chemical explosives encompass an array of nitroaromatic compounds (NACs), nitramines, nitrate esters, and peroxides [4]. Amidst these, the NACs are highly energetic explosives, which warrant sensitive and specific detection and therefore the prime concern of our work. Picric acid (PA) and trinitrotoluene (TNT) are utilized as primary and secondary explosives [5], with the explosive power of PA being superior than TNT [6]. PA is also used in battery, matches, and leather manufacturing units, rocket fuels processing, textile, fireworks, and dye industries [7–11]. Picric acid is a versatile compound and an embodiment of dual chemistry - one facet as an explosive and another as an antiseptic for treatment of burns, malaria, and smallpox [12–14] and an analytical reagent. Nevertheless, due to PA's high water-soluble character, soil and the aquatic system get contaminated instantaneously [15,16]. As per WHO [17], 0.001 mg L^{-1} is the permissible PA concentration in groundwater. Consistent long-term exposure to picric acid may affect the respiratory organ, red blood cell, kidney, liver, spleen, and nervous system [18,19]. Hence, chemists have a crucial task to fabricate new sensors for selective and sensitive detection of PA in the aqueous matrix, which will minimize cost, render a low limit of detection but maximize portability.

Widely used methodologies such as gas chromatography [20,21], surface plasmon resonance [22], thermal neutron analysis [23], SERS [24,25], X-ray imaging [26] etc., have been reported for efficient detection of PA. However, these techniques have limited practical applicability due to expensive instrumentation, lack of trained technicians, time-consuming calibration, intervention from other components, and poor sensitivity. In this regard, the self-assembly of simple fluorophore molecules for nitro explosive detection can be a viable approach. Such probes manifest high fluorescence quantum yields and enhanced sensitivity with remarkable electron-donating capacity, while the cognate analytes are electron-deficient explosives, which exhibit non-fluorescence properties [27,28]. Efficient π-π stacking between these molecules followed by intramolecular charge-transfer transition effectively suppresses self-quenching and could provide a unique molecular design for emissive organic self-aggregates. The donor-acceptor interaction phenomena via π-π interconnection and the strongest N–H

* Corresponding author.
E-mail addresses: aramesh@iitg.ac.in (A. Ramesh), gdas@iitg.ac.in (G. Das).

https://doi.org/10.1016/j.dyepig.2021.109779
Received 9 July 2021; Received in revised form 7 August 2021; Accepted 11 August 2021
Available online 2 September 2021

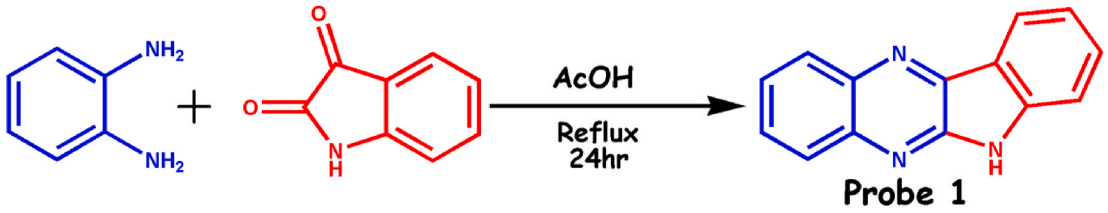

Scheme 1. Synthetic route of the **Probe 1** (6H-indolo [3,2-b]quinoxaline).

interaction with nitro explosives trigger luminescence quenching [29–31]. Hence, the development of self-assembled molecular probes that can engage in assembly-disassembly processes in the presence of PA and subsequently render ultra-trace detection of picric acid in a 100% aqueous matrix is our utmost concern. In light of this premise, we designed and synthesized a simple quinoxaline-based fluorescence self-aggregated probe for discriminative detection of PA in water via "*turn-off*" mode. The aforementioned self-assembled fluorescence sensor, which belongs to the family of small π-conjugated linear fluorophore, is scarce compare to widely explored naphthalimide, pyrene, thienylazulene, pyrazoline-based fluorescent aggregates [32–34] for recognition of PA. Owing to its high fluorescence quantum yield, simple single-step synthesis, better sensitivity with high K_{sv} value, the self-aggregated probe is suitable to recognize PA in complex samples i.e., soil and groundwater samples. Convenient low-priced, portable paper strips were also prepared for an instant, on-site detection of PA, devoid of sophisticated analytical equipments. The application potential of the developed probe is substantiated by detecting intracellular PA in live cell imaging studies.

2. Experimental section

2.1. Synthetic procedure of *probe 1* (6H-indolo [3,2-b]quinoxaline)

The synthesis of compound **Probe 1** (Scheme 1) was executed in 90% yield following a previously documented procedure [35]. **Probe 1** was characterized by HRMS, ^{1}H NMR, ^{13}C NMR, FTIR. The detailed synthetic method and associated spectroscopic investigations have been elaborated in the ESI (Figs. S1–S4, Supporting Information).

2.2. Photophysical characterisation studies

The photophysical characterization of **Probe 1** was performed in a pure aqueous medium. In the emission experiment, the excitation wavelength was chosen at 400 nm, while the emission spectra were recorded from 420 nm to 650 nm. The detailed experimental procedure for UV–visible and fluorescence spectroscopic analysis is mentioned in the ESI.

2.3. Preparation of portable test strips

Whatman filter paper (Whatman 42) was immersed into the solution of **Probe 1** (5×10^{-6} M) in DMSO and allowed to dry at room temperature. When the solvent evaporated completely, the **Probe 1** coated filter paper was cut into small portable test strips (2.0 cm × 1.0 cm) and then used for rapid on-site estimation of PA.

2.4. Cytotoxicity and cell imaging studies with *probe 1*

The experimental protocol followed for evaluating the cytotoxic potential of **Probe 1** and its application in cell imaging studies for detection of PA is mentioned in the Supporting Information.

3. Results and discussions

3.1. Photophysical investigation

The photophysical properties of **Probe 1** were explored in various solvents by UV–visible absorption and fluorescence spectroscopy at room temperature. For these studies, a 1.0 mM stock solution of **Probe 1**

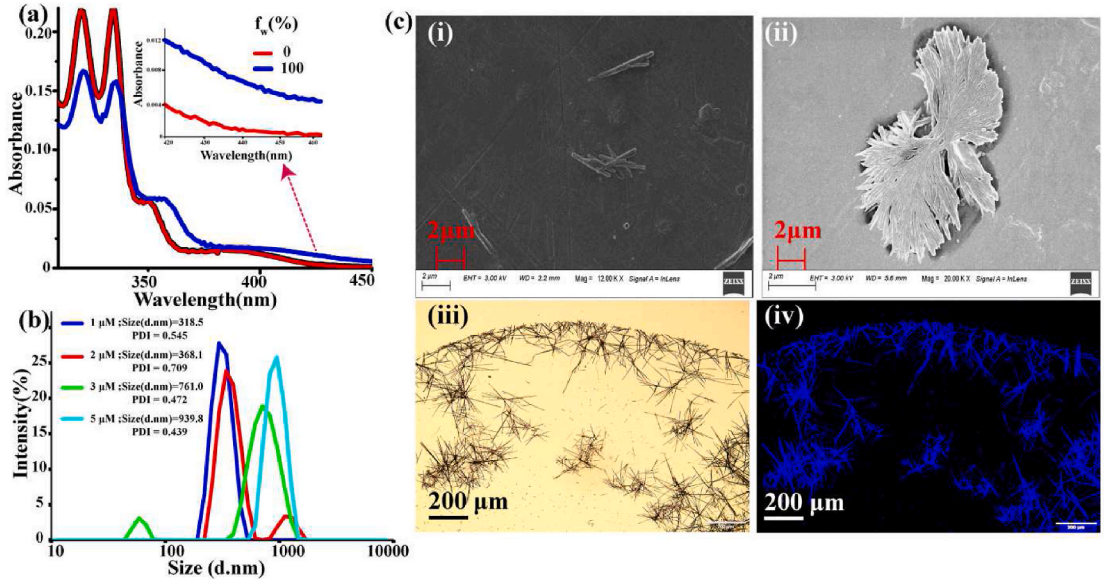

Fig. 1. (a) UV–visible spectra of **Probe 1** (5 μM) in different water fractions at room temperature. (b) DLS spectra of **Probe 1** for various concentrations in aqueous medium. (c) FESEM image for (i) 1.0 μM, (ii) 5.0 μM concentration of **Probe 1** and Fluorescence microscopy images for 5.0 μM **Probe 1**: (iii) Bright field (iv) Darkfield.

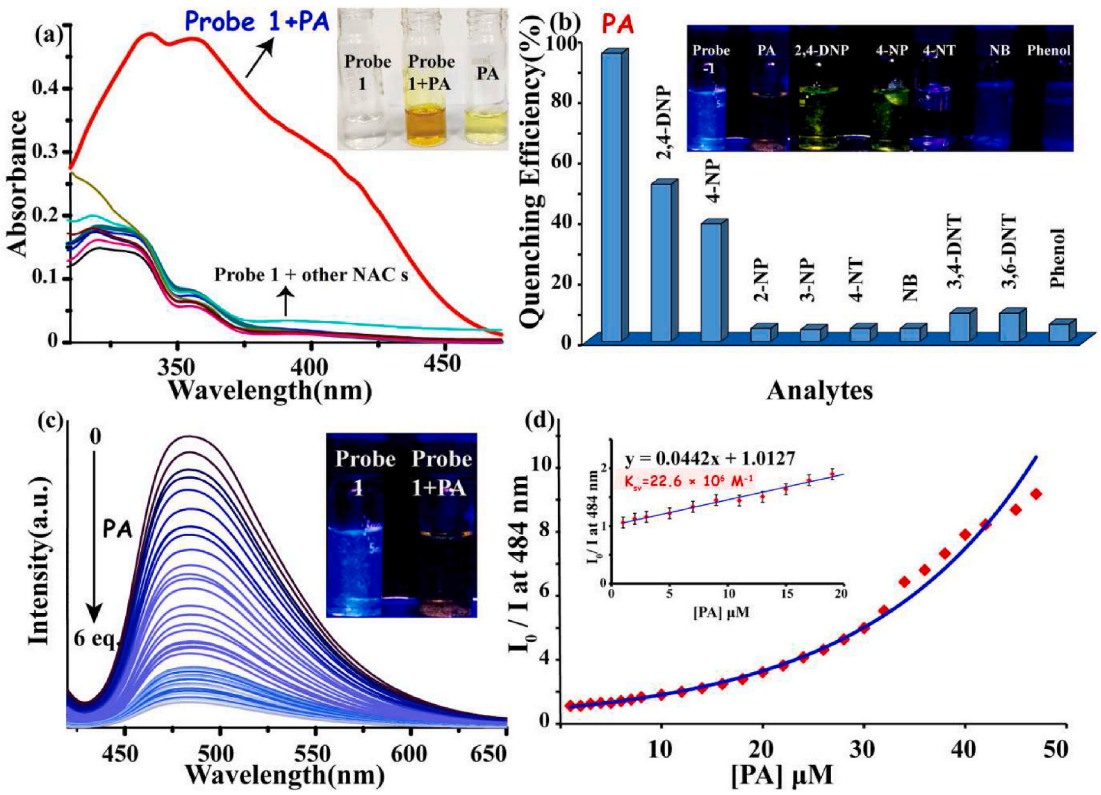

Fig. 2. (a) Absorption spectra of **Probe 1** (5.0 μM) in the presence of various NACs (50 Equiv) in aqueous medium; Inset: Visual color change of **Probe 1** solution in the presence of PA. (b) Fluorescence quenching efficiency (λ_{ex} = 400 nm) of **Probe 1** (5.0 μM) in water in the presence of various analytes (50 Equiv.). Inset: Visual change in fluorescence intensity of **Probe 1** observed under UV light upon addition of different analytes. (c) Change in fluorescence intensity of **Probe 1** (5.0 μM, λ_{ex} = 400 nm) upon incremental addition of PA. Inset: Visual color change of **Probe 1** in presence of PA. (d) Stern-Volmer plot: I_0/I vs. [PA]. Inset: Stern-Volmer plot achieved at a lower concentration of PA (0 μM–20 μM). (For interpretation of the references to color in this figure legend, the reader is referred to the Web version of this article.)

was prepared in dimethylsulfoxide (DMSO) and diluted consequently with the experimental solutions. The UV–visible spectra of **Probe 1** (5.0 μM) in pure acetonitrile and pure water is depicted in Fig. 1a. **Probe 1** manifested absorption bands at 321, 335, 351 nm and a hump at 383 nm in acetonitrile. In water, the absorption maxima were slightly right-shifted to 322, 337, 360 nm along with a broad hump around 410 nm, which can be assigned to π–π* electronic transitions [36] of quinoxaline moiety. Water content also reduced the intensity of absorption followed by a tailing beyond 440 nm, which can perhaps be ascribed to Mie scattering [37] owing to the presence of micro-aggregates in an aqueous solution. Nevertheless, naked-eye inspection suggested that the aqueous solution of **Probe 1** was transparent with no apparent precipitation.

The fluorescence spectra was recorded by varying the content of water in a solution of **Probe 1** in acetonitrile (Fig. S5a, Supporting Information). The fluorescence spectra of **Probe 1** in acetonitrile/water mixtures gave emission maxima between 460 and 462 nm. But upon enhancing the amount of water to 100%, the emission maxima with considerably reduced intensity was red-shifted to 484 nm. The redshift observed in the emission maxima suggested the transformation of a single probe molecule into a self-aggregated entity via intermolecular non-covalent interactions. This further confirmed the self-assembly of **Probe 1** molecule in presence of 100% water. The concentration-dependent fluorescence spectra of **Probe 1** in water also validated the rise in emission intensity upon self-assembly (Fig. S5b, Supporting Information). Furthermore, to validate the formation of aggregates, DLS and FESEM studies were also pursued in acetonitrile and aqueous medium. DLS study was accomplished in various concentrations ranging from 1.0 μM to 5.0 μM. The result indicated formation of self-aggregated **Probe 1** as the average hydrodynamic radius ranged from 318.5 nm to 939.8 nm with PDI 0.545 to 0.439 in the aqueous medium (Fig. 1b) whereas, in acetonitrile, no variation in hydrodynamic radius was observed. In an aqueous medium, variation in the hydrodynamic radius was observed due to efficient π-π interaction leading to self-assembled aggregate formation. In solution, π-π interaction influencing intermolecular aggregation phenomenon is well documented in the literature for polyaromatic planar molecules [38–40]. FESEM study indicated that **Probe 1** (5.0 μM) exhibited a propensity to self-assemble to generate leaf-like aggregates in pure water (Fig. 1c; i, ii). Fluorescence microscope images also confirmed the presence of self-aggregated **Probe 1** emitting bright blue fluorescence (Fig. 1c; iii, iv).

3.2. Sensing performance toward PA

The π electron-rich and strongly emissive nature of self-assembled **Probe 1** encouraged us to investigate its prospective application as a fluorescent chemosensor for nitroaromatics (NACs), which are likely to interact strongly with electron-rich self-aggregated fluorescent **Probe 1**. Further, it was conceived that owing to insufficient electron density in NACs, electron transfer would ensue smoothly between the fluorescent probe and electron-poor NACs resulting in the probe's rapid fluorescence quenching. To explore the self-aggregated probe's sensing ability towards nitroaromatics, we assessed the effect of various nitroaromatic compounds in aqueous medium. When an aqueous solution of **Probe 1** (5.0 μM) was treated with various NACs such as picric acid (PA), 2,4-dinitrophenol (2,4-DNP), 4-nitrophenol (4-NP), 3-nitrophenol (3-NP), 2-nitrophenol (2-NP), 4-nitrotolune (4-NT), 3,4-dinitrotolune (3,4-DNT), 3,6-dinitrotolune (3,6-DNT), nitrobenzene (NB) and non-nitro compound like sodium nitrite, phenol (Fig. S6, Supporting Information), the absorption spectra of **Probe 1** (ε = 30914.6 M^{-1} cm^{-1}) changed remarkably in the presence of only PA, indicating a strong

Table 1
A representative comparison of K_{sv} values and the detection limits along with the receptor and solvent system used for the detection of PA.

Sl No.	References	Receptor	Solvent System	LOD (ppb)	K_{sv} (M^{-1})
1.	**Present work**	Self-assembled Quinoxaline derivative	100% Aqueous medium	55.9	22.6×10^6
2.	Sensors and Actuators: B. Chemical., 2021, 330 129,287	Polyaromatic-based imidazolium	Aqueous medium	1145.5 (5 μM)	9.57×10^6
3.	Anal. Chem., 2019, 91, 13,675-13680	BODIPY probe	Acetonitrile/water (8:2) mixture	100 (0.44 μM)	Not reported
4.	Spectrochimica Acta Part A: Molecular and Biomolecular Spectroscopy, 2019, 223, 117,201	Coumarin based probe	Acetonitrile/water (1:9) mixture	2176.5 (9.5 μM)	2.21×10^5
5.	Dyes and Pigments, 2020, 181, 108,563	Tripodal naphthalimide derivative	DMF/H_2O (1 : 9, v/v) solution	10.83	73.6×10^3
6.	Sensors and Actuators B, 2017, 250, 215–223	Lanthanide complexes	Aqueous medium	114.5 (0.5 μM)	8.553×10^4
7.	J. Am. Chem. Soc. 2017, 139, 2421-2427	Conjugated Covalent Organic Frameworks	Dichloromethane	Not reported	Not reported
8.	J. Am. Chem. Soc., 2016, 138, 3302–3305	Pyrene-based self-assembly	DMF	Not reported	3.1×10^4
9	J. Fluoresc. 2016, 26, 395-401	Perylene diimide derivatives	DMF	229.1	Not reported
10.	RSC Adv. 2016, 6, 84,319-84325	Arcridine derivatives	MeOH	549.84	1.8×10^4

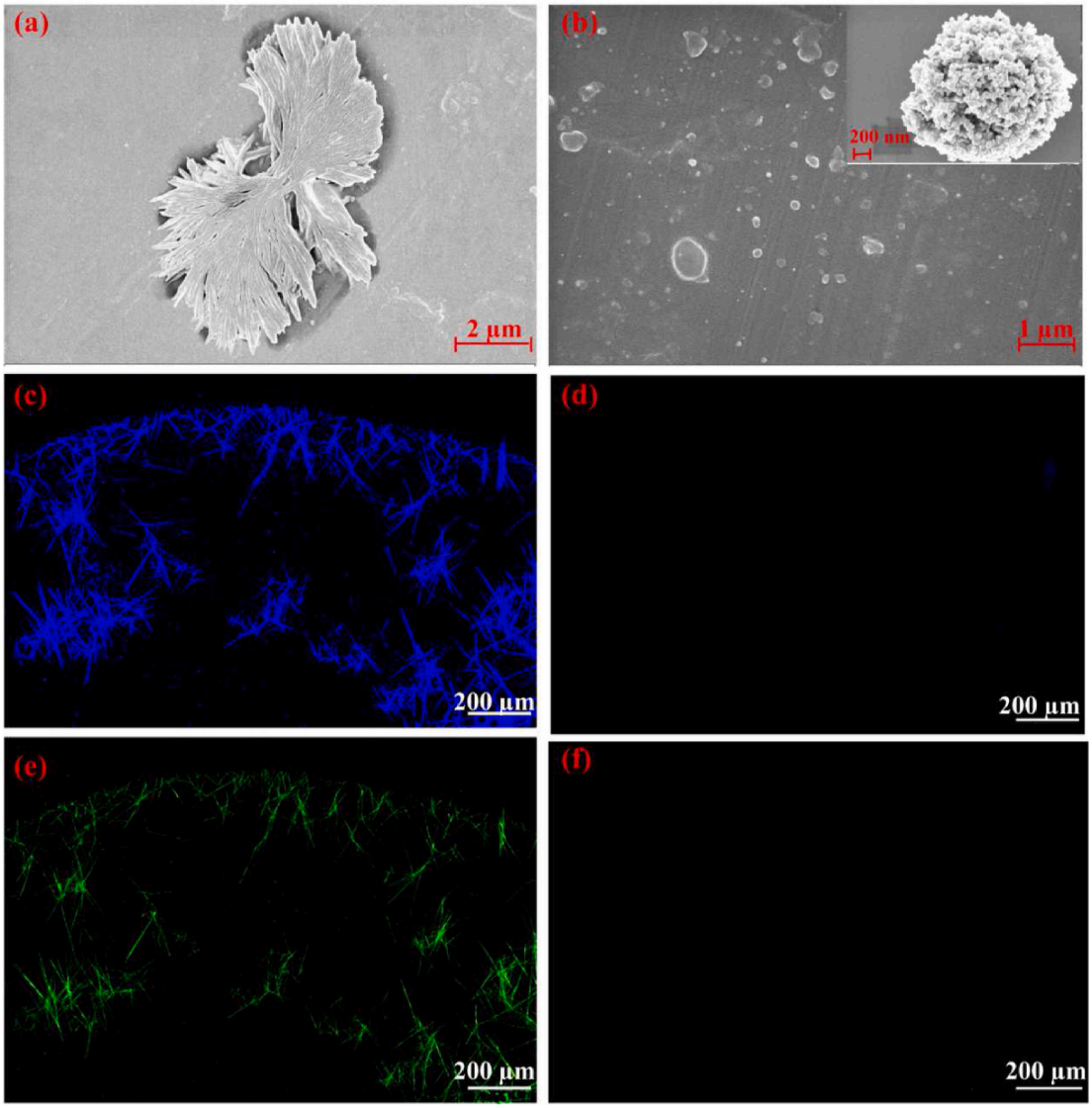

Fig. 3. FESEM and Fluorescence microscope images of **Probe 1** (5.0 μM) (a, c and e), **Probe 1** + PA (b; Inset: Magnified view, d, and f) in 100% aqueous medium.

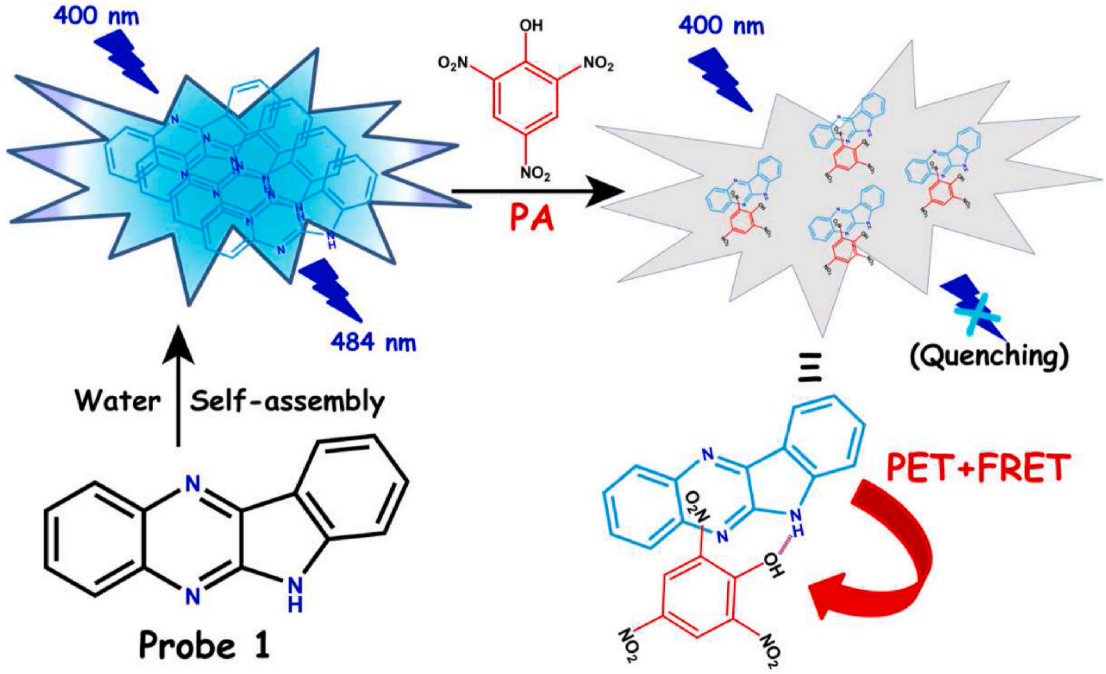

Scheme 2. Schematic representation of the proposed binding model for self-assembled **Probe 1** and PA.

interaction between PA and **Probe 1** ($\varepsilon = 98697.4\ M^{-1}\ cm^{-1}$) (Fig. 2a). Further, the visual appearance of **Probe 1** in solution changed immediately from colorless to mustard yellow, possibly due to the formation of the charge-transfer complex.

The fluorescence spectra of self-assembled **Probe 1** (5.0 μM, Quantum yield = 0.91) manifested an intense emission maxima at 484 nm when excited at 400 nm in an aqueous solution. Surprisingly, after the addition of various NACs and non-nitro compounds, prominent quenching was observed in the case of nitrophenol solutions, while the others revealed minimal changes. A significant quenching of emission (~95%) was observed upon addition of 6 Equiv. of PA, while for 2,4-DNP and 4-NP, quenching efficiency was only 51% and 38%, respectively (Fig. 2b). As the number of nitro groups increased, electron deficiency enhanced in NACs, and electron drifts were elevated from the electron-rich sensor to NACs followed by strong intermolecular interactions, leading to a higher extent of fluorescence quenching. Consequently, with the addition of PA, the quenching efficiency was maximum (Quantum yield = 0.087) as compared to other nitroaromatics, suggesting the selectivity of self-aggregated **Probe 1** toward PA. Since nitrophenols displayed substantial quenching among all other NACs, fluorescence titration experiments with only PA (Fig. 2c), ,4-DNP and 4-NP were pursued. For these three nitrophenols, the emission intensity of **Probe 1** decreased with the incremental addition of the analyte. The quenching mechanism was also evaluated by Stern-Volmer (SV) equation. The SV plot was found to be linear at a lower concentration of PA with a Stern-Volmer constant (K_{sv}) of $22.6 \times 10^6\ M^{-1}$ (Fig. 2d, inset), which is more significant than earlier reported values in the literature [41], while at a higher concentration of PA, the plot was apparently exponential (Fig. 2d). The linear response at lower concentration of PA and a high K_{sv} value may be ascribed to static quenching, while the non-linear nature at higher concentration of PA signified the involvement of dynamic quenching in presence of an additional energy transfer process [42]. Interestingly, K_{sv} values for 2,4-DNP and 4-NP were lower than the K_{sv} value for PA ($22.6 \times 10^6\ M^{-1}$) and was estimated to be 4.26×10^6 and $1.68 \times 10^6\ M^{-1}$, respectively with a linear response plot (Figs. S7 and S8, Supporting Information). Hence, the K_{sv} values could render discrimination amongst PA, DNP, and NP. To illustrate the mechanistic aspect of fluorescence quenching, time-resolved fluorescence spectra of **Probe 1** (5.0 μM, $\lambda_{ex} = 400$ nm) in an aqueous medium was recorded before and after the addition of PA. Both the time-resolved decays were fitted to bi-exponential decay along with a significantly decreased lifetime from 3.85 ns to 1.52 ns upon addition of PA (Table S1, Supporting Information). The decrease in lifetime with the gradual addition of PA signified a dynamic quenching mechanism, i.e., diffusion-controlled collision [43] between the excited sensor and the quencher. The limit of detection [44] for PA was calculated to be ~56 ppb (Fig. S9, Supporting Information) using an earlier reported procedure in the literature [45]. The K_{sv} and LOD obtained for the probe for PA detection in the current study compares well with previous reports (Table 1). The limit of quantification (LOQ) for PA was estimated to be 186 ppb (Fig. S9, Supporting Information). The interference and selectivity studies with other NACs, common cations and anions (2,4-DNP; 4-NP, 2-NP, 3-NP, 4-NT, NB, 3,4-DNT, 3,6-DNT, phenol, Fe^{3+}, Al^{3+}, Cr^{3+}, Hg^{2+}, Cd^{2+}, Pb^{2+}, Cu^{2+}, Co^{2+}, Ni^{2+}, Zn^{2+}, Ca^{2+}, Mg^{2+}, PO_4^{3-}, Cl^-, I^-, $H_2PO_4^-$, HSO_4^-, NO_3^-, OH^-, HSO_3^-, HCO_3^-, SH^-, oxalate^{2-}) were also examined. Their effect on sensitivity and selectivity of **Probe 1** for PA was very negligible (Fig. S10, Supporting Information).

FESEM analysis and fluorescence microscopic studies were conducted to ascertain the variation in surface morphology of self-assembled **Probe 1** in the absence and presence of PA. Self-assembled **Probe 1** exhibited leaf-like morphology, which became smaller and displayed round-shaped morphology upon interaction with PA (Fig. 3a and b). In fluorescence microscope analysis, the intense fluorescence emitted by the self-assembled probe was completely dissipated upon interaction with PA (Fig. 3c–f). Conceivably, interaction with PA resulted in disaggregation of the self-assembled **Probe 1**. This tenet was corroborated by DLS studies, wherein the self-assembled **Probe 1** displayed a higher hydrodynamic radius (939.8 nm) as compared to **Probe 1**-PA complex (353.7 nm) (Fig. S11, Supporting Information), strongly suggesting dissociation of the self-assembled **Probe 1**. In order to gain further insight into the sensing phenomenon (Scheme 2), Job's plot was generated, which indicated that **Probe 1**-PA formed a 1:1 stoichiometric complex (Fig. S12, Supporting Information). HRMS studies further verified the complexation between **Probe 1** and PA. (Fig. S13, Supporting Information). Additionally, ^{1}H NMR study (Fig. S14, Supporting

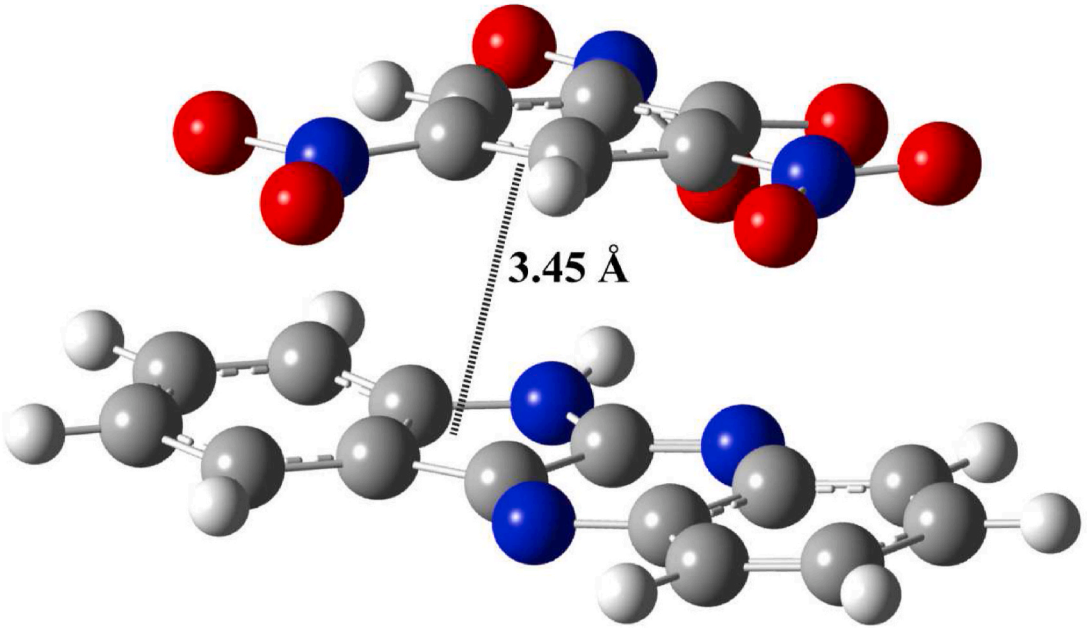

Fig. 4. Optimized geometry of **Probe 1**-PA ensemble.

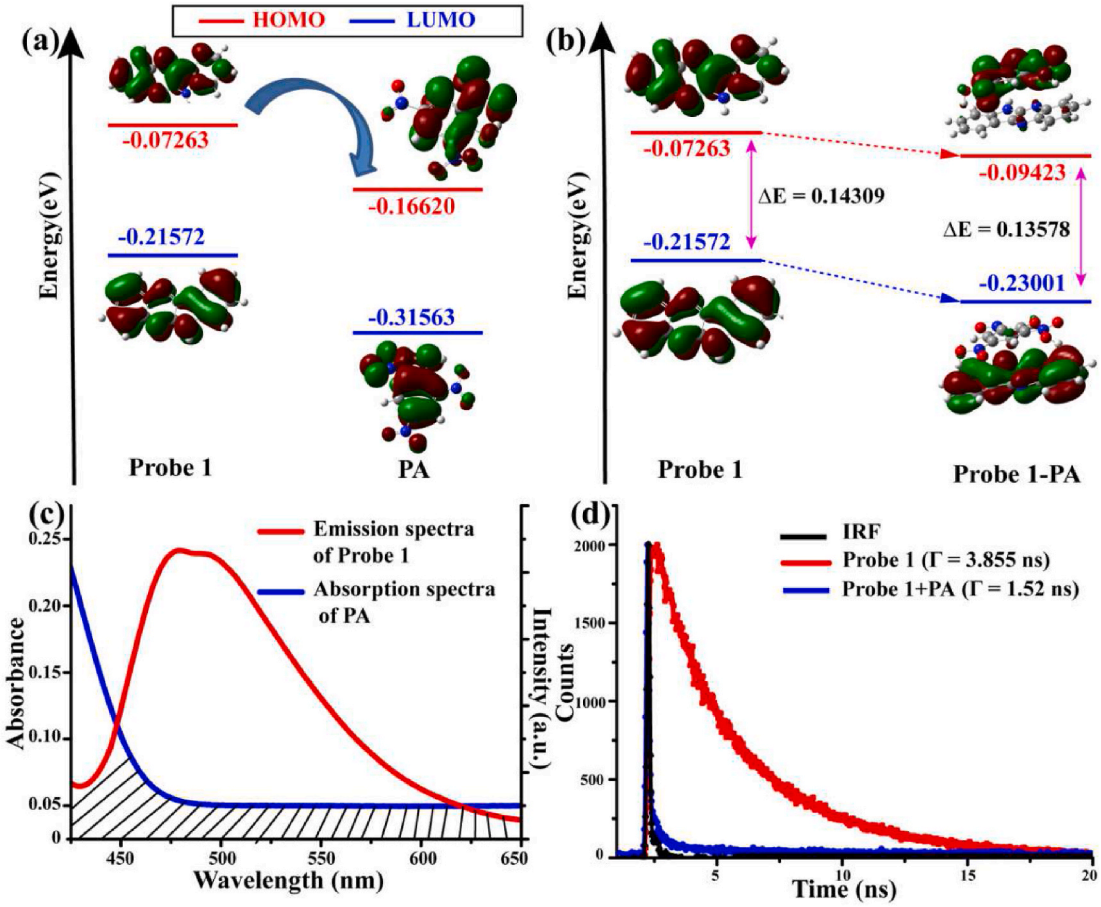

Fig. 5. (a) Graphical representation of the suggested photoinduced electron transfer (PET) from LUMO of **Probe 1** to LUMO of PA. (b) Relative energy levels (HOMO and LUMO) of **Probe 1** and **Probe 1**-PA. (c) Spectral overlap of the emission spectra of **Probe 1** (red line) and the absorption spectra of PA (blue line) in the aqueous medium. (d) Time-resolved fluorescence spectra of **Probe 1** (5.0 μM) and in the presence of PA. (For interpretation of the references to color in this figure legend, the reader is referred to the Web version of this article.)

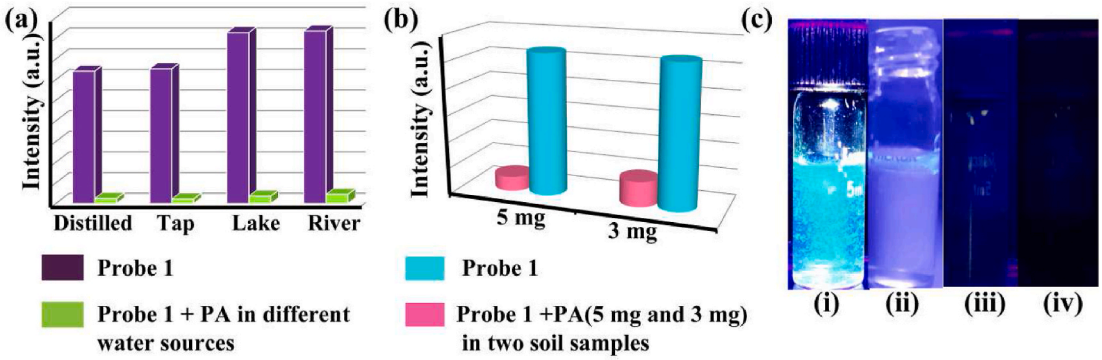

Fig. 6. (a) Changes in emission intensity of **Probe 1** (5.0 μM) at 484 nm in the presence of excess PA in natural sources of water. (b) Emission spectra of **Probe 1** for detecting PA in real soil specimens (5.0 mg and 3.0 mg). (c) The visual appearance of PA in soil samples under 365 nm UV illumination (i) Only **Probe 1** (5.0 μM) (ii) **Probe 1** (5.0 μM) with 50 mg of soil but devoid of PA (iii) **Probe 1** (5.0 μM) with 50 mg of soil with 3 mg and 5 mg of PA respectively.

Information) was also carried out, which revealed that the N–H proton's signal was downfield shifted (Δδ = 0.233 ppm) along with a slight downfield shift of aromatic protons of **Probe 1** upon addition of 1 Equiv. PA [46].

This kind of ^{1}H NMR signal pattern might be ascribed to the complexation possibility between **Probe 1** and PA due to probable hydrogen bonding between N–H with phenolic –OH in PA, which was further verified by the DFT-optimized structure of **Probe 1**-PA (Fig. 4) where the shortest hydrogen bonding distance between these two moieties was found to be 3.23 Å and the average plane distance between **Probe 1** and the benzene ring of PA was around 3.45 Å [47,48].

3.3. Quenching mechanism of PA sensing

To investigate the fluorescence "*turn-off*" mechanism of **Probe 1** with PA, density functional theory (DFT) calculations were accomplished with the B3LYP/6–31 G (d, p) method basis set using the Gaussian 09 program [49]. The optimized geometry (Fig. 4) and the highest occupied molecular orbital (HOMO), and the lowest unoccupied molecular orbital (LUMO) of **Probe 1** and **Probe 1**-PA complex are depicted in Fig. 5. In general, when an electron-rich fluorophore interacts with an electron-deficient species, there will be facile photoinduced electron transfer (PET) from LUMO of the excited fluorophore to the LUMO of the NACs followed by reverse electron transfer to the HOMO of the probes in a non-radiative process leading to the extinction of the emission intensity of the fluorophore. Hence the DFT results confirmed that there is a probability of PET from **Probe 1** LUMO (−0.07263 eV) to the PA LUMO (−0.16620 eV) (Fig. 5a), which was also assisted by static quenching, i.e., the generation of non-fluorescent ground state complex as evident from the S–V plot [50]. LUMO levels of 2,4-DNP (−0.13879 eV) and 4-NP (−0.02944 eV) are usually higher than LUMO of PA, resulting in lower efficiency of fluorescence quenching. In comparison to other nitro explosives such as 2-NP (−0.00913 eV), 3-NP (−0.00864 eV), and NB (−0.02452 eV), the PA LUMO energy level is the lowest; consequently, the effect of quenching was insignificant for them (Fig. S15, Supporting Information) [51]. The energy difference between the HOMO and LUMO of the **Probe 1**-PA ensemble (0.13578 eV) dropped compared to that of **Probe 1** (0.14309 eV), indicating that the complexation of **Probe 1**-PA is energetically more favorable (Fig. 5b). In addition to PET, small spectral overlap (Fig. 5c) ensued between the emission spectra of self-assembled **Probe 1** and UV–visible spectra of PA along with the variation in the fluorescence decay time of **Probe 1** after the addition of PA (Fig. 5d). So, it is plausible that FRET may account for fluorescence quenching to some extent and established the dynamic quenching mechanism too. As reported in previous publications [52], it is conspicuous that self-aggregated **Probe 1** displayed excellent selectivity and sensitivity towards PA due to concomitant occurrence of PET and FRET [53] from the electron enriched **Probe 1** to the electron-scarce PA, which resulted in the noteworthy "*turn-off*" luminescence emission among all NACs.

3.4. Detection of PA in natural water samples, soil samples, and bio-fluid samples

Following a military operation, water and soil pollution by PA is very common, and overexposure to PA (above 20 ppm) could be hazardous. To authenticate the suitability of **Probe 1** it was pertinent to ascertain whether the probe could detect PA in groundwater samples in presence of common anions and metal ions. Lake water and river water specimens were brought from the Serpentine lake (IIT Guwahati Campus) and

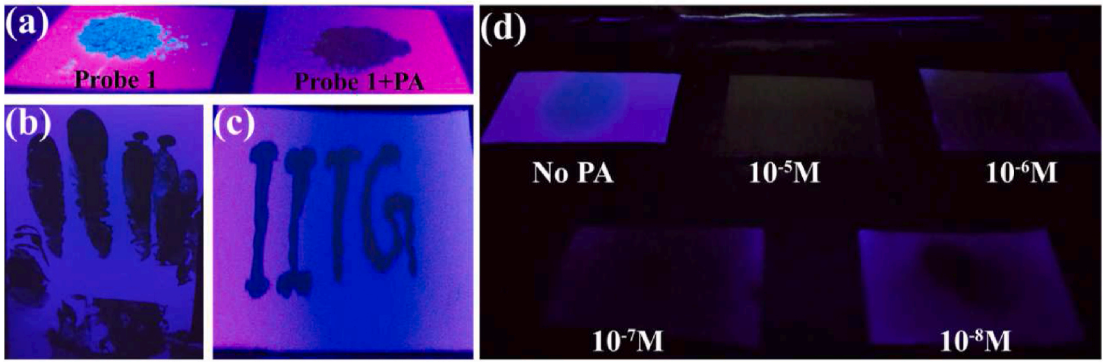

Fig. 7. (a) Visual appearance of solid **Probe 1** powder before and after addition of PA under 365 nm UV illumination. (b) Quenched luminescence of PA exposed handprint on **Probe 1** coated white paper. (c) Photograph of quenched fluorescence on contact mode. (d) Visual detection of **Probe 1** (5 μM) coated test strips before and after adding different PA concentrations under 365 nm light.

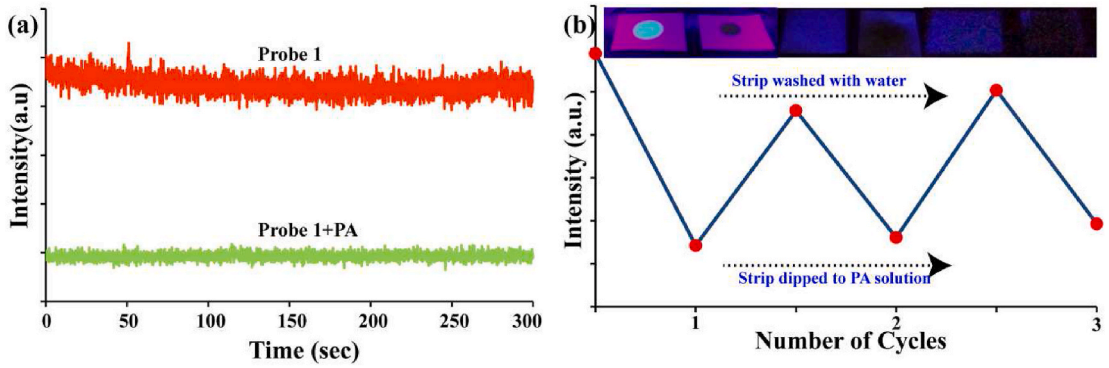

Fig. 8. (a) Change in fluorescence intensity of **Probe 1** and **Probe 1**-PA by varying exposure time. (b) Reusability test of **Probe 1**.

Brahmaputra river (near IIT Guwahati Campus). Tap water was available in the laboratory. These water samples were initially centrifuged at 10,000 rpm for 5 min and then filtered using a 0.22 μm membrane filter to separate any particulate matter. Subsequently, fluorescence spectroscopic studies with **Probe 1** was carried out with these real water samples for detection of PA according to the previously reported literature [54]. The fluorescence spectra of **Probe 1** (5.0 μM) displayed emission maxima at 484 nm in real water samples, and showed approximately similar quenching efficiency (Fig. 6a) as that of distilled water when PA was added to the solution without any significant interference from common ions. The results of the quantitative recovery of spiked specimens of analyte is shown in Table S2.

For on-site practical implementation of **Probe-1** for PA sensing, we also widened our investigation by using soil specimen [55]. Soil samples were accumulated from IIT Guwahati campus garden. A 1.0 g sample of fine-grained crushed soil was taken in two separate petri dishes. Next, 5.0 mg and 3.0 mg of PA were combined with two different soil samples individually and blended thoroughly. The soil sample devoid of PA was considered as blank. Finally, 50 mg soil sample from each was added to the aqueous solution of **Probe 1** (5.0 μM), each solution was filtered, and fluorescence was recorded wherein similar quenching behavior was observed (Fig. 6b). The sample containing **Probe 1** and only soil without PA exhibited high fluorescence intensity (Fig. 6c), suggesting the usefulness of the self-aggregated **Probe 1** for excellent PA detection in the soil. Another practical utility of **Probe 1** for detecting PA was explored by varying the pH, i.e., in three different simulated bio-fluid samples instead of water. Interestingly, the outcome revealed that **Probe 1** was able to recognize PA in the simulated body fluid (pH~7.4), gastric fluid (pH ~2.0), and intestinal fluid (pH ~8.0) by rendering distinguishable "*turn-off*" fluorescence changes (Supporting Information, Fig. S16).

3.5. Contact mode estimation of PA

The contact mode analysis was executed by rubbing few crystals of PA on the right hand (nitrile gloved) and pressing onto a white paper. The paper was already coated with fine particles of **Probe 1**. Finally, the paper was exposed to UV light to detect trace amount of PA. PA exposure was evident from the quenching of the emission when the samples were irradiated with the UV lamp (Fig. 7a–c).

3.6. Paper-based detection of PA

Following solution-phase detection of PA successfully, our subsequent goal was to pursue contact mode detection of PA, which would

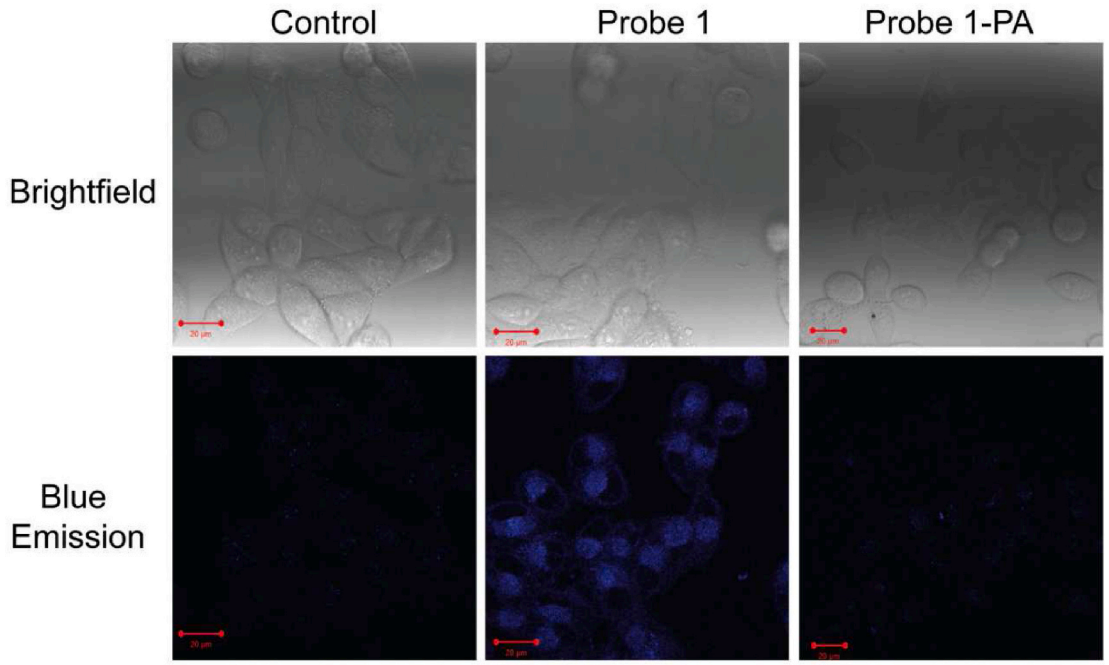

Fig. 9. Confocal microscope-based fluorescence images of HeLa cells treated with 10 μM of **Probe 1** alone and HeLa cells pre-treated with 10 μM of **Probe 1** followed by addition of 10 μM PA solution. Scale bar for the images is 20 μm.

render beneficial implications in forensic and analytical research. The prepared filter paper test strips described in the experimental section were selected for PA detection. A small amount of freshly prepared PA solution (10^{-5} - 10^{-8} M) was applied to the test strips, and a dark spot appeared in every case after visualizing under a hand-held 365 nm UV light (Fig. 7d). According to the previously reported methods [56], in order to determine the minimum detection limit of **Probe 1** solution soaked test strips, 10 μL volume from 10^{-8} M stock PA solution (22.9 pg PA) was applied on the test strips, which covered a surface area of about 1 cm^2. The detection limit for these paper strips was 22.9 pg cm^{-2} for naked eye PA recognition. The initial fluorescence intensity of **Probe 1** as well as **Probe 1**-PA ensemble was found to be retained as a function of increasing exposure time (Fig. 8a).To investigate the reusability of the **Probe 1** coated paper strips, the strips were washed with distilled water and dried in oven. Emission intensity of the washed and dried strips were recorded and the whole process was repeated three times (Fig. 8b). Therefore, these experiments and images demonstrate the utility and sensitivity of **Probe 1** coated paper strips for instant and repeated visual detection of trace amount of PA.

3.7. Live cell imaging for detection of PA

Based on the positive results obtained in solution and filter strip-based PA detection, it was envisaged that **Probe 1** could be leveraged in fluorescence-based live cell imaging studies for the detection of intracellular PA. In order to pursue this objective, it was critical to initially ascertain the cytotoxic potential of **Probe 1**. An *in vitro* MTT assay revealed that **Probe 1**, **Probe 1**-PA complex (1:1 complex) as well as PA alone used at a concentration ranging from 2.5 μM–10 μM was not detrimental to the viability of HeLa cells (cell viability in excess of 80%) (Fig. S17, Supporting Information), which indicated that **Probe 1** as well as **Probe 1**-PA complex was essentially non-toxic at these tested concentrations. This finding was encouraging and it motivated us to ascertain the prospect of **Probe 1** in detecting intracellular PA by fluorescence-based cell imaging. In this context, HeLa cells alone failed to exhibit any fluorescence (Fig. 9, control panel), whereas a bright blue fluorescence emission was associated with HeLa cells incubated with **Probe 1** when visualized under UV excitation (Fig. 9, ligand panel). It may be mentioned here that the localization of the blue fluorescence emission in HeLa cells incubated with **Probe 1** appeared to be cytoplasmic in nature. Interestingly, when HeLa cells were pre-treated with **Probe 1** and then incubated with PA, a dramatic quenching of the intracellular fluorescence was observed (Fig. 9, ligand-PA panel). It was also noted that the distinctive morphology of HeLa cells was retained during the imaging studies, which substantiated the non-toxic nature of **Probe 1** and its suitability in detecting intracellular PA.

4. Conclusions

In summary, we report the synthesis of a small quinoxaline-based **Probe 1** for effective and selective fluorescence-based detection of PA over other NACs in aqueous solution, natural water samples, solid and paper-based systems. Due to π-π stacking interaction, **Probe 1** spontaneously self-assembled in an aqueous solution to leaf-like aggregates, which was disrupted to smaller round-shaped aggregates in presence of PA. FESEM study, fluorescence microscopic analysis along with DLS investigation corroborated the aggregation-disaggregation process. Based on the experimental evidence, disaggregation of the self-assembled sensor, and PET, FRET is concomitantly responsible for the discriminative detection of PA in water with high selectivity and sensitivity. Self-aggregated **Probe 1** manifested high selectivity and good sensitivity towards PA as the K_{SV} was 22.6×10^6 M^{-1} and LOD was ~56 ppb. Paper-based detection for PA was achieved at the picogram level, enabling rapid and real on-site detection. The developed probe could also be employed in imaging studies for non-invasive fluorescence-based sensing of PA in live HeLa cells. Based on its non-toxic nature, it is envisaged that the probe can bear interesting prospect in future as a non-destructive imaging handle for PA detection in *in vivo* cellular system.

CRediT authorship contribution statement

Megha Basak: Conceptualization, Methodology, Investigation, Writing-Original draft, preparation. **Basu Bhattacharjee:** Methodology, Investigation. **Aiyagari Ramesh:** Writing- Reviewing and Editing. **Gopal Das:** Supervision, Conceptualization, Writing- Reviewing and Editing.

Declaration of competing interest

The authors declare that they have no known competing financial interests or personal relationships that could have appeared to influence the work reported in this paper.

Acknowledgments

The financial support by DBT (BT/COE/34/SP28408/2018, BT/PR13560/COE/34/44/2015 and BT/PR41449/NER/95/1687/2020) and DST (SR/FST/CS-II/2017/23C) New Delhi, India, is highly acknowledged. The author also thanks the Central Instruments Facility (CIF), IIT Guwahati, for providing the necessary facilities. MB is thankful to Asesh Das, Department of Chemistry and Deepa Sachan, Centre for the Environment, IIT Guwahati, for their generous help. The authors thank the Centre for Nanotechnology, IIT Guwahati and Debashree Debasmita for assisting in confocal microscope analysis. MB and BB acknowledge IIT Guwahati for a research fellowship.

Appendix A. Supplementary data

Supplementary data to this article can be found online at https://doi.org/10.1016/j.dyepig.2021.109779.

References

[1] Germain ME, Knapp MJ. Optical explosives detection: from color changes to fluorescence turn-on. Chem Soc Rev 2009;38:2543–55.
[2] Li YJ, Zhang YF, Zhang YM, Wang ZH, Yang HL, Yao H, Wei TB, Lin Q. Tripodal naphthalimide assembled novel AIE supramolecular fluorescent sensor for rapid and selective detection of picric acid. Dyes Pigments 2020;181:108563.
[3] Yinon J. Detection of explosives by Mass Spectrometry in Counterterrorist detection techniques of explosives. Elsevier B.V.; 2007.
[4] Murray L. Fed Regist 2010;75(229):73935–4604.
[5] Madhu S, Bandela A, Ravikanth M. BODIPY based fluorescent chemodosimeter for explosive picric acid in aqueous media and rapid detection in the solid state. RSC Adv 2014;4:7120–3.
[6] Akhavan J. The chemistry of explosives. Royal Society of Chemistry; 2011.
[7] Acharyya K, Mukherjee PS. A fluorescent organic cage for picric acid detection. Chem. Commun. 2014;50:15788–91.
[8] Xu Y, Li B, Li W, Zhao J, Sun S, Pang Y. ICT-not-quenching"near infrared ratiometric fluorescent detection of picric acid in aqueous media. Chem. Commun. 2013;49:4764–6.
[9] Roy B, Bar AK, Gole B, Mukherjee PS. Fluorescent tris-imidazolium sensors for picric acid explosive. J Org Chem 2013;78:1306–10.
[10] Guo R, Jiao T, Li R, Chen Y, Guo W, Zhang L, Zhou J, Zhang Q, Peng Q. Sandwiched Fe3O4/carboxylate graphene oxide nanostructures constructed by layer-by-layer assembly for highly efficient and magnetically recyclable dye removal. ACS Sustainable Chem Eng 2018;6:1279–88.
[11] Geng R, Chang R, Zou Q, Shen G, Jiao T, Yan X. Biomimetic nanozymes based on coassembly of amino acid and hemin for catalytic oxidation and sensing of biomolecules. Small 2021;17:2008114.
[12] Venkatramaiah V, Kumar S, Patil S. Fluoranthene based fluorescent chemosensors for detection of explosive nitroaromatics. Chem, Commun. 2012;48:5007–9.
[13] Xie W, Zhang SR, Du DY, Qin JS, Bao SJ, Li J, Su ZM, He WW, Fu Q, Lan YQ. Stable luminescent metal-organic frameworks as dual-functional materials to encapsulate Ln3+ ions for white-light emission and to detect nitroaromatic explosives. Inorg Chem 2015;54:3290–6.
[14] Peng Y, Zhang AJ, Dong M, Wang YW. A colorimetric and fluorescent chemosensor for the detection of an explosive-2,4,6-trinitrophenol (TNP). Chem. Commun. 2011;47:4505–7.

[15] Yao Y, Xue M, Chen J, Zhang M, Huang F. An amphiphilic pillar[5]Arene: synthesis, controllable self-assembly in water, and application in calcein release and TNT adsorption. J Am Chem Soc 2012;134:15712–5.
[16] Adil LR, Gopikrishna P, Krishnan Iyer P. Receptor-free detection of picric acid: a new structural approach for designing aggregation-induced emission probes. ACS Appl Mater Interfaces 2018;10:27260–8.
[17] Environmental Protection Agency. Innovative treatment technologies: Annual status report. eighth ed. 1996. EPA-542- R-96-010.
[18] Wollin KM, Dieter HH. Toxicological guidelines for monocyclic nitro-, amino- and aminonitroaromatics, nitramines, and nitrate esters in drinking water. Arch Environ Contam Toxicol 2005;49:18–26.
[19] Hussain S, Malik AH, Afroz MA, Iyer PK. Ultrasensitive detection of nitroexplosive – picric acid via a conjugated polyelectrolyte in aqueous media and solid support. Chem. Commun. 2015;51:7207–10.
[20] Walsh ME. Determination of nitroaromatic, nitramine, and nitrate ester explosives in soil by gas chromatography and an electron capture detector. Talanta 2001;54:427–38.
[21] Qian C, Wang R, Li M, Li X, Ge B, Bai Z, Jiao T. Facile preparation of self-assembled black phosphorus-based composite LB films as new chemical gas sensors. Colloids Surf, A 2021;608:125616.
[22] Byram C, Moram SSB, Shaik AK, Soma VR. Versatile gold based SERS substrates fabricated by ultrafast laser ablation for sensing picric acid and ammonium nitrate. Chem Phys Lett 2017;685:103–7.
[23] Vourvopoulos G, Womble PC. Pulsed fast/thermal neutron analysis: a technique for explosives detection. Talanta 2001;54:459–68.
[24] Hakonen A, Wang F, Andersson PO, Wingfors H, Rindzevicius T, Schmidt MS, Soma VR, Xu S, Li Y, Boisen A, Wu H. Hand-held femtogram detection of hazardous picric acid with hydrophobic Ag nanopillar SERS substrates and mechanism of elasto-capillarity. ACS Sens 2017;2:198–202.
[25] Wang R, Yan X, Ge B, Zhou J, Wang M, Zhang L, Jiao T. Facile preparation of self-assembled black phosphorus-dye composite films for chemical gas sensors and surface-enhanced Raman scattering performances. ACS Sustainable Chem Eng 2020;8:4521–36.
[26] Brown KE, Greenfield MT, McGrane SD, Moore DS. Advances in explosives analysis - Part II: photon and neutron methods ABC highlights: authored by rising stars and top experts. Anal Bioanal Chem 2016;408:49–65.
[27] Sharma S, Dubey G, Sran BS, Bharatam PV, Hundal G. Fabrication of a hydrazone-based Al(III)-Selective "turn-on" fluorescent chemosensor and ensuing potential recognition of picric acid. ACS Omega 2019;4:18520–9.
[28] Wang L, Cui M, Tang H, Cao D. Fluorescent nanoaggregates of quinoxaline derivatives for highly efficient and selective sensing of trace picric acid. Dyes Pigments 2018;155:107–13.
[29] Balakrishnan K, Datar A, Zhang W, Yang X, Naddo T, Huang J, Zuo J, Yen M, Moore JS, Zang L. Nanofibril self-assembly of an arylene ethynylene macrocycle. J Am Chem Soc 2006;128:6576–7.
[30] Liu T, Ding L, Zhao K, Wang W, Fang Y. Single-layer assembly of pyrene end-capped terthiophene and its sensing performances to nitroaromatic explosives. J Mater Chem 2012;22:1069–77.
[31] Bhalla V, Gupta A, Kumar M, Rao DSS, Prasad SK. Self-assembled pentacenequinone derivative for trace detection of picric acid. ACS Appl Mater Interfaces 2013;5:672–9.
[32] Lin HH, Chan YC, Chen JW, Chang CC. Aggregation-induced emission enhancement characteristics of naphthalimide derivatives and their applications in cell imaging. J Mater Chem 2011;21:3170–7.
[33] Itami K, Ohashi Y, Yoshida JI. Triarylethene-based extended π-systems: programmable synthesis and photophysical properties. J Org Chem 2005;70:2778–92.
[34] An BK, Kwon SK, Jung SD, Park SY. Enhanced emission and its switching in fluorescent organic nanoparticles. J Am Chem Soc 2002;124:14410–5.
[35] Dowlatabadi R, Khalaj A, Rahimian S, Montazeri M, Amini M, Shahverdi A, Mahjub E. Impact of substituents on the isatin ring on the reaction between isatins with ortho-phenylenediamine. Synth Commun 2011;41:1650–8.
[36] Marin L, Lutsen L, Vanderzande D, Maes W. Quinoxaline derivatives with broadened absorption patterns. Org Biomol Chem 2013;11(35):5866–76.
[37] Zhao J, Ji S, Chen Y, Guo H, Yang P. Excited state intramolecular proton transfer (ESIPT): from principal photophysics to the development of new chromophores and applications in fluorescent molecular probes and luminescent materials. Phys Chem Chem Phys 2012;14:8803–17.
[38] Mukherjee S, Desai AV, Inamdar AI, Manna B, Ghosh SK. Selective detection of 2,4,6-trinitrophenol (TNP) by a π-stacked organic crystalline solid in water. Cryst Growth Des 2015;15:3493–7.
[39] Shetty AS, Zhang J, Moore JS. Aromatic π-stacking in solution as revealed through the aggregation of phenylacetylene macrocycles. J Am Chem Soc 1996;118:1019–27.
[40] Markova LI, Malinovskii VL, Patsenker LD, Häner R. J- vs. H-type Assembly: pentamethine cyanine (Cy5) as a near-IR chiroptical reporter. Chem. Commun. 2013;49:5298–300.
[41] Das G, Biswal BP, Kandambeth S, Venkatesh V, Kaur G, Addicoat M, Heine T, Verma S, Banerjee R. Chemical sensing in two dimensional porous covalent organic nanosheets. Chem Sci 2015;6:3931–9.
[42] Pramanik B, Singha N, Das D. Sol-, gel-, and paper-based detection of picric acid at femtogram level by a short peptide gelator. ACS Appl. Polym. Mater. 2019;1:833–43.
[43] Liu J, Zhong Y, Lu P, Hong Y, Lam JWY, Faisal M, Yu Y, Wong KS, Tang BZ. A superamplification effect in the detection of explosives by a fluorescent hyperbranched poly(silylenephenylene) with aggregation-enhanced emission characteristics. Polym Chem 2010;1:426–9.
[44] Pinrat O, Boonkitpatarakul K, Paisuwan W, Sukwattanasinitt M, Ajavakom A. Glucopyranosyl-1,4-Dihydropyridine as a new fluorescent chemosensor for selective detection of 2,4,6-trinitrophenol. Analyst 2015;140:1886–93.
[45] Pherkkhuntod C, Ervithayasuporn V, Chanmungkalakul S, Wang C, Liu X, Harding DJ, Kiatkamjornwong S. Water-soluble polyaromatic-based imidazolium for detecting picric acid: pyrene vs. Anthracene. Sensor Actuator B Chem 2021;330:129287.
[46] Vijayakumar C, Tobin G, Schmitt W, Kim MJ, Takeuchi M. Detection of explosive vapors with a charge transfer molecule: self-assembly assisted morphology tuning and enhancement in sensing efficiency. Chem. Commun. 2010;46:874–6.
[47] Jiang K, Luo SH, Pang CM, Wang BW, Wu HQ, Wang ZY. A functionalized fluorochrome based on quinoline-benzimidazole conjugate: from facile design to highly sensitive and selective sensing for picric acid. Dyes Pigments 2019;162:367–76.
[48] Shylaja A, Rubina SR, Roja SS, Kumar RR. Novel blue emissive dimethylfuran tethered 2-aminopyridine-3-carbonitrile as dual responsive fluorescent chemosensor for Fe^{3+} and picric acid in nanomolar detection limit. Dyes Pigments 2020;174:108062.
[49] Fisch M, Trucks G, Schlegel H, Scuseria G, Robb M, Cheeseman J, Scalmani G, Barone V, Mennucci B, Petersson G. Gaussian 09 (Revision A. 02). 2009. Wallingford, CT.
[50] Meher N, Iyer PK. Pendant chain engineering to fine-tune the nanomorphologies and solid state luminescence of naphthalimide AIEEgens: application to phenolic nitro-explosive detection in water. Nanoscale 2017;9:7674–85.
[51] Martínez-Máñez R, Sancenón F. Fluorogenic and chromogenic chemosensors and reagents for anions. Chem Rev 2003;103:4419–76.
[52] Kartha KK, Babu SS, Srinivasan S, Ajayaghosh A. Attogram sensing of trinitrotoluene with a self-assembled molecular gelator. J Am Chem Soc 2012;134:4834–41.
[53] Malik AH, Hussain S, Kalita A, Iyer PK. Conjugated polymer nanoparticles for the amplified detection of nitro-explosive picric acid on multiple platforms. ACS Appl Mater Interfaces 2015;7:26968–76.
[54] Kumari S, Joshi S, Cordova-Sintjago TC, Pant DD, Sakhuja R. Highly sensitive fluorescent imidazolium-based sensors for nanomolar detection of explosive picric acid in aqueous medium. Sensor Actuator B Chem 2016;229:599–608.
[55] Kaja S, Damera DP, Nag A. A metal-enhanced fluorescence sensing platform for selective detection of picric acid in aqueous medium. Anal Chim Acta 2020;1129:12–23.
[56] Xiong JF, Li JX, Mo GZ, Huo JP, Liu JY, Chen XY, Wang ZY. Benzimidazole derivatives: selective fluorescent chemosensors for the picogram detection of picric acid. J Org Chem 2014;79:11619–30.